



New insights into “dead lithium” during stripping in lithium metal batteries

Xiao-Ru Chen^a, Chong Yan^a, Jun-Fan Ding^b, Hong-Jie Peng^c, Qiang Zhang^{a,*}

^a Beijing Key Laboratory of Green Chemical Reaction Engineering and Technology, Department of Chemical Engineering, Tsinghua University, Beijing 100084, China

^b Advanced Research Institute of Multidisciplinary Science, School of Materials Science and Engineering, Beijing Institute of Technology, Beijing 100081, China

^c Department of Chemical Engineering, Stanford University, Stanford, CA 94305, USA

ARTICLE INFO

Article history:

Received 27 February 2021

Revised 25 March 2021

Accepted 25 March 2021

Available online 6 April 2021

Keywords:

Lithium metal batteries

Dead lithium

Lithium stripping

Lithium dendrite growth

Charge transfer

ABSTRACT

Lithium (Li) metal attributes to the promising anode but endures the low Columbic efficiency (CE) and safety issues from the inactive Li accumulation. The metallic Li which is isolated from the lithium anode (named dead Li⁰) consists the major component of the inactive Li. We systematically and meticulously investigated the formation and evaluation of dead Li⁰ during stripping process from electron transfer, the oxidation of Li⁰ to Li⁺ and the diffusion of Li⁺ through solid electrolyte interphase (SEI). The above-mentioned processes were regulated by adjusting the contact sites of electron channels, the dynamic rate of conversion from Li⁰ to Li⁺, and the structure as well as components of SEI. The design principles for achieving less dead Li⁰ and higher CE are proposed as a proof of concept in lithium metal batteries. This new insight sheds a comprehensive light on dead Li⁰ formation and guides the next-generation safe batteries for future application.

© 2021 Science Press and Dalian Institute of Chemical Physics, Chinese Academy of Sciences. Published by ELSEVIER B.V. and Science Press. All rights reserved.

1. Introduction

The target of carbon-neutral and net-zero emissions drive the highly efficient and sustainable conversion and storage of renewable energy [1]. The safe energy storage systems are essential to utilize renewable energy and achieve cleaner environment [2,3]. Lithium (Li) metal with a theoretical capacity of 3860 mAh g⁻¹ and an electrode potential of -3.04 V versus standard hydrogen electrode is highly recognized as the eternal promising alternative anode for next-generation rechargeable batteries [4–8].

Nevertheless, the major issue of Li metal batteries (LMBs) is the low Coulombic efficiency (CE) [9,10], indicating the limited cycle life before batteries stop working [11–15]. The low CE in LMBs is attributing from the fact that the active Li converted into the inactive Li, which consists of the Li components in solid electrolyte interphase (SEI) and SEI-wrapped metallic Li (dead Li⁰) [16–18]. Specifically, the SEI will undergo damage and re-generate due to the huge volume deformation of Li metal anode as the continue conversion between Li⁺ and Li⁰ [19,20]. Consequently, the SEI layer grows into thicker and more non-uniform, exacerbating the volume deformation of Li anode in turn. At the same time, the non-uniform SEI accelerates the uneven Li stripping. The thick SEI and

uncontrollable Li stripping will result in the wrapping of metallic Li by SEI [21]. The above-mentioned evolution process can ultimately increase the consumption of active Li caused by the SEI formation [22–24]. Besides, the SEI-wrapped metallic Li generated on the anode will not only significantly aggravate the diffusion barrier of Li ions and render high overpotential as well as rapid capacity fade, but also bring about huge security risks due to the very high reactivity of Li metal [25,26]. Further discriminating the origin of active Li is the key to inhibiting the capacity decay while improving the CE of LMBs.

The low CE is chiefly attributed to the constantly growth of SEI [27–30]. This is helpful to understand the stability of SEI and afford various emerging method to achieve stable SEI layer of lithium metal. However, it is difficult to quantitatively distinguish the consumption proportion between SEI and dead Li⁰. Although a lot of effective strategies have been proposed to modify and control the SEI [31,32]. The intrinsic correlation between the modified SEI and constantly consumptive active Li is unclear. Meanwhile, the low CE with LMBs is still not completely solved especially after long-term cycling. Recently, Meng and co-workers promoted an emerging method to first accurately measure the amount of inactive Li and considered that the dead Li⁰ was the dominant factors bringing about the low CE with LMBs [33]. Therefore, figuring out the formation and evolution of the dead Li⁰ is the precondition to fundamentally enhance the CE of LMBs. Accordingly, some

* Corresponding author.

E-mail address: zhang-qiang@mails.tsinghua.edu.cn (Q. Zhang).

efforts have been made to investigate the evolution of dead Li⁰. For instance, Dasgupta and co-workers demonstrated that the dead Li⁰ concentrated on the Li metal anode introduced a tortuous pathway for Li⁺ transport and thereby increased in total electrode overpotential [34]. Xu et al. developed a physics-based model to understand how dead Li⁰ affects the apparent capacity loss in LMBs [35]. Tewari et al. found that the amount of dead Li⁰ formed during stripping increased with decreasing current and increasing temperatures via a synergistic computational and experimental approach [36]. The systematic understanding of dead Li⁰ formation during stripping process is scarce but essential to suppress dead Li⁰ formation for the safer and longer-lifespan LMBs [37,38].

In this contribution, the formation and evaluation of dead Li⁰ was systematically and meticulously investigated during stripping process from electron transfer, the oxidation of Li⁰ into Li⁺ and the diffusion of Li⁺ through SEI [35,39]. Concretely, when maintaining the electron channels on Li anode, the recovered dead Li⁰ and less dead Li⁰ formation can be achieved via modifying the contact sites of electron channels. The higher rate of conversion from Li⁰ to Li⁺ renders chaotic Li stripping, while the more amount of dead Li⁰ is formed. The Li⁺ diffusion in SEI is subsequently controlled and the extraordinary SEI composed by faster Li⁺ conductor guarantees less dead Li⁰ formation. This work affords a comprehensive understanding of dead Li⁰ formation that guides the design principles to enable less dead Li⁰ and higher CE of future LMBs.

2. Experimental

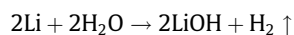
2.1. Materials

The Li metal foils (500 μm) were purchased from the China Energy Lithium Co., Ltd. The 1,2-dimethoxyethane (DME), 1,3-dioxolane (DOL), and Li bis(trifluoromethanesulfonyl)imide (LiTFSI) were provided by Tokyo Chemical Industry Co., Ltd. The Lithium nitrate (LiNO₃) was bought from Shanghai Aladdin Bio-Chem Technology Co., Ltd. Copper foil, Poly tetra fluoroethylene (PTFE) rings, and Celgard 2400 polypropylene (PP) membranes were purchased from Shenzhen Kejing Star Technology Co., Ltd. The electrolyte of DD was 1.0 M LiTFSI in DOL/DME (v:v = 1:1) and DD-N was DD with 5wt% LiNO₃. All materials were preserved and adopted in a glove box with O₂ and H₂O contents below 1.0 ppm.

2.2. Materials characterization

The JSM 7401F scanning electron microscope (SEM) and the JEM 2010 transmission electron microscope (TEM) were utilized to observe the morphology of the samples. The samples were protected in Ar in a home-made container to avoid the sample contacting with air during transfer process before characterization. The Cu foil in half cell after cycles was washed carefully with DME to fully remove residual Li salt and other impurities. The amount of metallic Li is monitored through Titration gas chromatography (TGC). The detail steps of TGC are: (1) the as-detected electrode disassembled from coin cell and put into a headspace bottle in glove box, (2) 0.5 mL H₂O injected into the headspace bottle, (3) 5 mL gas in the headspace bottle transferred into the gas chromatography (GC) after reaction and shacking, (4) the area of H₂ peak obtained, and (5) the amount of Li⁰ gained from the as-established H₂ calibration curve. The calibration curve was plotted and fitted though the seven sample of as-measured metallic Li (0.56, 1.04, 1.23, 1.46, 1.91, 2.77, and 3.07 mg) and the corresponding area of H₂ peak from GC. A shimadzu GC-2014 Tracera equipped with a thermal conductivity detector was employed to measure the amount of H₂, which

can be used to calculate the amount of Li metal based on the following reaction:



2.3. Electrochemical measurement

2.3.1. In-situ observation of Li plating/stripping

A homemade optical cell with quartz window was employed to in-situ observant [40,41]. Li foil and Cu wire were adopted as the counter electrode and working electrode, respectively. The Cu wire was 3.0 cm in length and 0.01 cm in diameter. The DD electrolyte was used in the cells. The in-situ observation in this contribution was carried out under a microscope and recorded by a charge coupled device camera. The Solartron 1470E electrochemical workstation (Solartron Analytical, UK) was utilized for galvanostatic Li plating and stripping. The homemade optical cell was observed at 5.3 mA cm⁻² with a capacity of 0.44 mA h cm⁻² for every Li plating/stripping process.

2.3.2. Half cell assemble and electrochemical measurements

Half cells were assembled using a Cu foil and a Li metal foil as electrodes, and a Celgard 2400 PP membrane as the separator. In order to relieve the pressure in particle cell, a PTFE ring was placed between Celgard 2400 PP membrane and Cu foil, which could be specified in the main manuscript. The diameter of Cu foil was 13.0 mm. The thickness and diameter of Li metal foil were 500 μm and 16.0 mm, respectively. The outside and inside diameters of the PTFE ring were 14.0 and 16.0 mm, respectively.

The as-assembled half cells were monitored in galvanostatic mode using a Land CT2001 multichannel battery tester. The cells were firstly discharged with the capacity of 2.0 mA h cm⁻² at a given current density of 1.0, 2.0, 5.0 or 10.0 mA cm⁻² and then charged until the voltage reached 1.0 V at the current density of 1.0, 2.0, 5.0 or 10.0 mA cm⁻².

3. Results and discussion

The in-situ optical microscope (OM) was employed to monitor the formation of dead Li⁰ during repeated Li plating/stripping. The Li is quickly extracted from several active sites on the Cu wire at 5.3 mA cm⁻² with a capacity of 0.44 mA h cm⁻². Obviously, the final morphology of Li plating is rugged accompanied by local bulges and caves (Fig. 1a and e). During the subsequent 1st stripping process (Movie S1), the whole outline of Li deposition is almost constant with the morphology after 1st plating. Even in the images with higher magnification as Fig. 1f revealed, the more precise contour of Li deposition after 1st plating and 1st stripping is the same, suggesting the large amount of inactive Li reserved and low CE of LMBs. Meanwhile, there are several local active sites where local stripping rates are faster as shown the naked Cu wire in red circle (Fig. 1b). During the 2nd plating, the Li metal draws out from the root of origin electrode (Movie S2). The inactive Li formed during 1st stripping process is jacked up by the new Li deposition as shown in the yellow outline (Fig. 1b and c). The inactive Li which is accumulated on the surface of anode severely hinders the transmission of Li ions and therefore leads to the more serious uneven Li deposition in the following each cycle [35,42,43]. Beside of root-growth, the tip growth can be observed on the working Li metal anode (Fig. 1g) because these sites retain the electron channels with the anode. The behavior of the 2nd stripping step is similar with the 1st stripping step (Movie S3). The constant morphology after 2nd stripping compared with the morphology after 2nd plating demonstrates abundant inactive Li formed during stripping process.

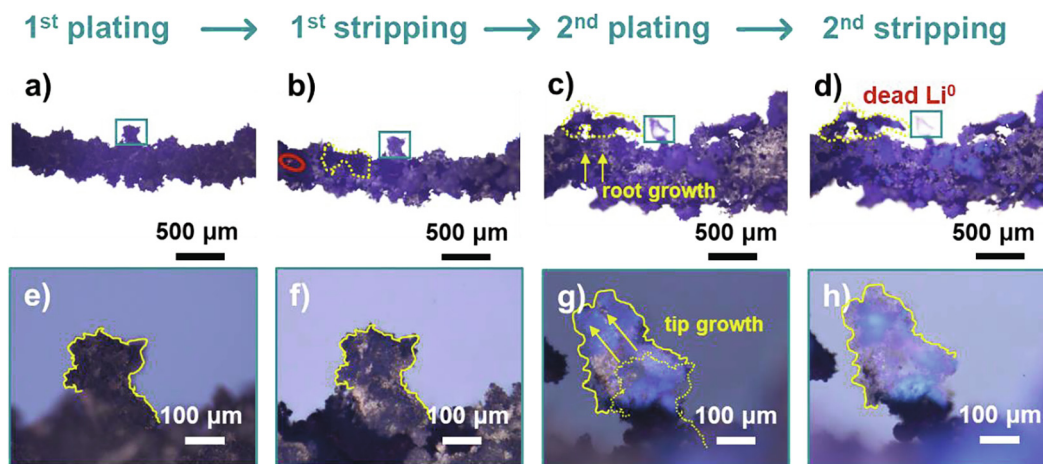


Fig. 1. The morphology of Li metal anode through in-situ optical microscope with the current density of 5.3 mA cm^{-2} with the capacity of $0.44 \text{ mA h cm}^{-2}$ after (a, e) 1st plating, (b, f) 1st stripping, (c, g) 2nd plating and (d, h) 2nd stripping. (e, f, g, and h) High magnification of Li deposition in blue area drawn in (a, b, c, and d), respectively.

Based on the above observation, inactive Li is formed during stripping process and accumulated on the electrode surface at the subsequent cycles, which is harmful for the battery performance and safety (Fig. 2a). In order to further explore the structure and components of inactive Li, TEM was employed to investigate the Li plating and stripping behavior after 1st cycle at the current density of 1.0 mA cm^{-2} with a capacity of 2.0 mA h cm^{-2} . The lattice fringe spacing of domains indicates the contribution of metallic Li (Fig. 2b), suggesting the metallic Li unreacted during the 1st stripping process. Both Li_2O and Li_2CO_3 can be identified through the lattice plane distance as shown in the Fig. S1, which is the importance component of the SEI layer. The TGC was further utilized to measure the amount of dead Li^0 from the area of H_2 peak area. As the Fig. 2d shown, the peaks of H_2 reacted from H_2O and the Cu foil after 1st cycle with 1.0 mA cm^{-2} are at 2.65 min and the area of H_2 peak is 24624. The area ratio of peaks at 3.82 min and 5.81 min is 1:3 and these two peaks also appear in the air sample. Herein the two peaks can be assumed as leaked O_2 and N_2 in air. The as-established H_2 calibration curve and equation are dis-

played in Fig. S2. Based on the equation of H_2 calibration curve, the capacity of dead Li^0 can be measured as 0.337 mAh precisely while the capacity of inactive Li is 0.538 mAh from the voltage-time curves during Li plating and stripping process. Hence, SEI components retain the capacity of 0.201 mAh and the dead Li^0 is the main component in inactive Li.

The dead Li^0 is directly formed during the stripping process because the partial metallic Li cannot immediately convert into Li^+ but is wrapped by insulated SEI [44–50]. The stripping processes involve the following stages: the electron transfer in solid phase, conversion of the Li atom to the Li^+ and Li^+ diffusion through SEI [51,52]. The detailed investigations of each stage will be exhibited in the further contribution.

The key factor of dead Li^0 formation is blocked electron transfer. To recover the electron channel between dead Li^0 and anode, the external force was applied to the anode with some inactive Li after five cycles at different current density with 2.0 mA h cm^{-2} per cycle (Fig. 3a). The anode accumulates the irreversible capacity of 5.61 mAh cm^{-2} after five cycles at the current density of

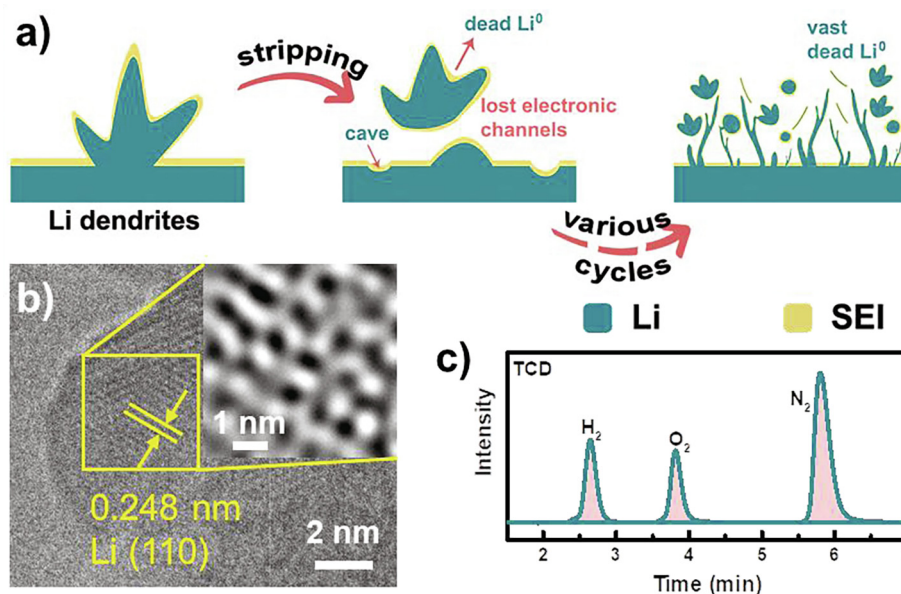


Fig. 2. (a) The scheme of dead Li^0 formation during Li stripping process. (b) TEM images of Cu foil after 1st Li plating/stripping (inside: Fourier-transformed crystalline lattice). (c) GC chromatogram of reaction gases with H_2 after H_2O titration on Cu foil after 1st plating/stripping.

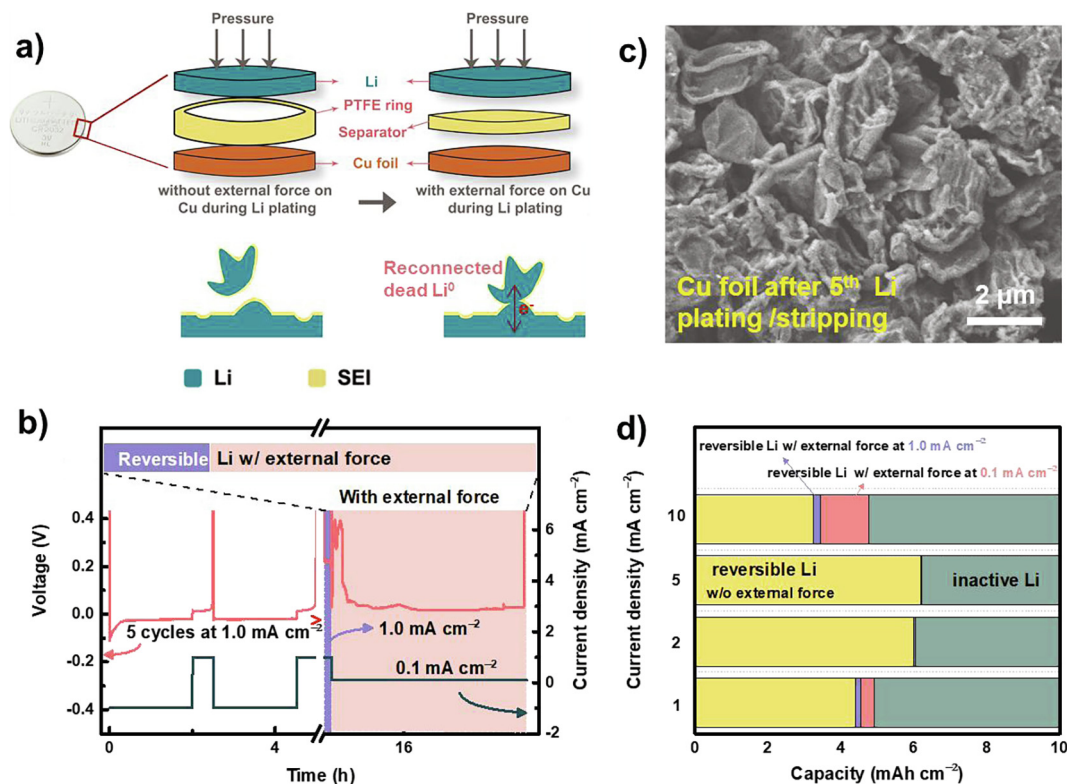


Fig. 3. (a) The scheme of coin cell with and without the external force on Cu foil. The external force adopted on Li anode after several cycles can push the partial dead Li⁰ to recover into active Li. (c) The SEM image of Cu foil after 5th Li plating/stripping with abundant inactive Li. (b) The voltage/current density – time curves with and without external force and (d) the corresponding fractions of Li composed from reversible Li, recovered Li and inactive Li at the current density of 1.0, 2.0, 5.0 and 10.0 mA cm⁻².

1.0 mA cm⁻² (Fig. 3b). The irreversible capacity of Li mainly comes from the formation of dead Li⁰, which can be observed through the SEM (Fig. 3c). When the external force applied, the anode subsequently exhibits the revived capacity of 0.14 mA h cm⁻² at 1.0 mA cm⁻² and continues to release a revived capacity of 0.37 mAh cm⁻² at reduced current density of 0.1 mA cm⁻² (Fig. 3d). When the current density increased to 2.0, 5.0, and 10.0 mA cm⁻² during cycles, the revived capacity can also appear under the function of external force (Fig. S3). The external force can rupture the partial SEI around the dead Li⁰ and above the Li anode. The dead Li⁰ with cracked SEI will revive due to the renewable electron channels linked under the function of external force. Therefore, when constructing more electron channels, the active Li will be guaranteed ceaseless electron transfer and converted into Li⁺ largely during stripping process (Fig. 3a). The carbon papers (CPs) are adopted as the Li hosts to ensure abundant electron channels. As a result, the diameter of a CP is 8.04 and 8.26 μm at the initial and 1st cycle, suggesting the Li wrapping a CP during plating process and removing from a CP totally as the function of more electron channels during stripping process (Fig. S4). Similar achievements made by Li host have been also found in some literatures [53–60], which is because of not only the reduced local current density but also the increased electron channels through our model experiments. The constant and sufficient electron channels are the necessary condition for more reversible Li⁰ reaction during Li stripping process and less dead Li⁰ formation.

The conversion rate of the Li atom to Li⁺ depends on the stripping current density. A series of stripping current density from 1.0 to 10.0 mA cm⁻² at the same plating current density with a plating capacity of 2.0 mAh cm⁻² in the Li | Cu half cells were employed to adjust the conversion rate. Fig. 4a demonstrates that their average CE of initial 30 cycles (the Li stripping capacity/Li plating capacity during initial 30 cycles) range from 48.72% to

92.21%. The average CE reduces as the stripping current density reducing under the same plating current density, suggesting the faster conversion rate results in lower CE and more inactive Li (Fig. S5). Besides, when changing the plating current density, the average CE almost steadies under the same stripping current density. This indicates that the CE is more corresponding with the stripping rate not the plating rate (Fig. S6). Therefore, more targeted strategies for controlling Li stripping process are essential to reduce the dead Li⁰ formation as well as improve the CE. When the cells last until 50 cycles, the average CE during initial 50 cycles still obeys the abovementioned principles (Fig. S7). The amount of dead Li⁰ is further measured through TGC and the results demonstrate that the capacity of dead Li⁰ is 0.837, 0.876, 1.332, and 1.561 mA h cm⁻² at the stripping current density of 1.0, 2.0, 5.0 and 10.0 mA cm⁻² after 5th cycle (Fig. 4b). The capacity of dead Li⁰ has a linear relationship with the accumulated inactive capacity during the initial 5 cycles (Fig. S8). The cumulative dead Li⁰ continues to increase the battery safety risks during cycles, while the higher stripping current density will deteriorate battery performance of the more dead Li⁰ forming.

To further explore the Li⁺ diffusion in the SEI during stripping process, 5% LiNO₃ is added into the DD electrolyte (1.0 M LiTFSI in DOL/DME (v:v = 1:1)), which can be donated DD-N electrolyte. The DD-N electrolyte will construct the uniform SEI with high ionic conductivity [61,62]. This is because the SEI formed in DD-N contains abundant Li components with high Li⁺ conductivity, such as Li₃N and Li_xO_y, which have been verified in the previous publications [40,63,64]. The evenner and higher conductive SEI achieves the ordered Li⁺ diffusion from every position of the surface of anode (Fig. 5a). Therefore, the average CE in DD-N during initial 30 cycles are 98.3%, 98.3%, 98.4%, and 67.8% at the same plating current density of 1.0 mA cm⁻² and the stripping current density of 1.0, 2.0, 5.0, and 10.0 mA cm⁻², separately, which are significantly higher

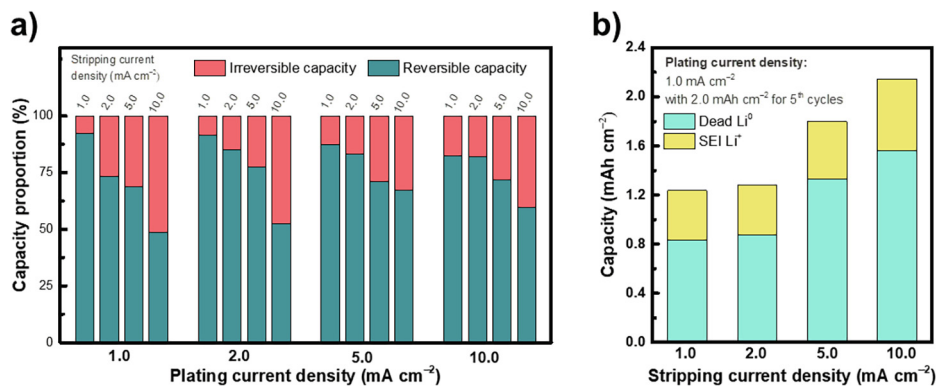


Fig. 4. (a) The average CE during the initial 30 cycles of Li | Cu half cells at a series of plating current density and stripping current density of 1.0, 2.0, 5.0 and 10.0 mA cm⁻². (b) TGC analysis capacity usage (dead Li⁰ and SEI Li⁺) after 5 cycles at the 1.0 mA cm⁻² plating current density and different stripping current density.

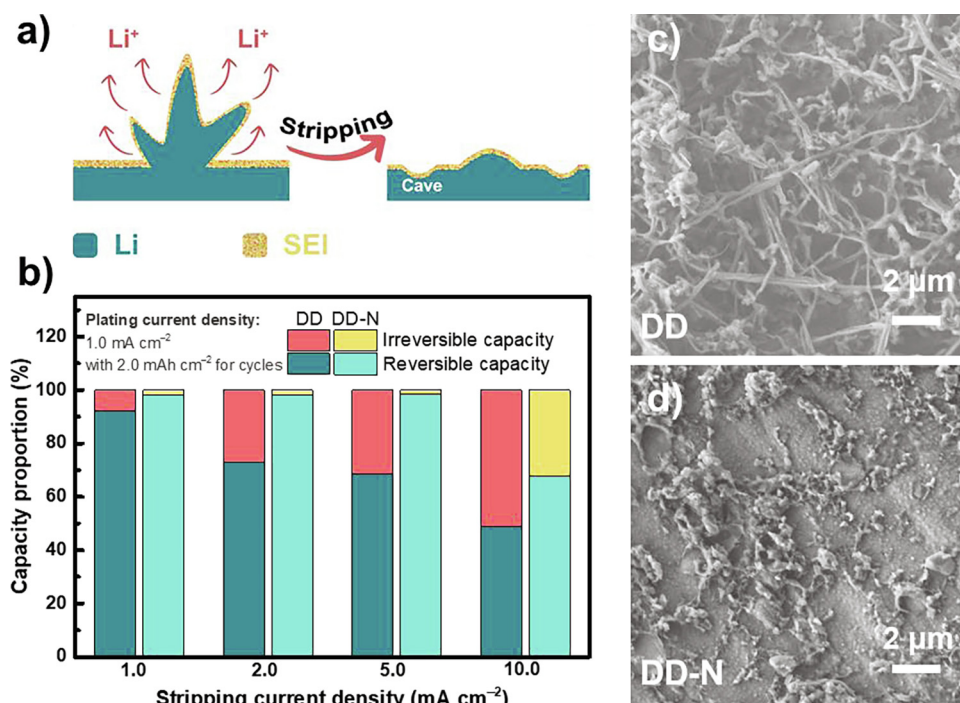


Fig. 5. (a) The schematic diagram of Li stripping process under the SEI with higher Li⁺ conductivity. (b) The average CE during the initial 30 cycles of Li | Cu half cells at 1.0 mA cm⁻² plating current density and different stripping current density with DD and DD-N electrolyte. The SEM images of Cu foils after 1st Li plating/stripping process at 1.0 mA cm⁻² with (c) DD electrolyte and (d) DD-N electrolyte.

compared with DD electrolyte (Fig. 5b and S9). The morphology of Li anode using the DD-N electrolyte after 1st cycle can further certificate the less dead Li⁰ forming under the function of ordered Li⁺ diffusion (Fig. 5c and d). The ordered Li⁺ diffusion from the surface of anode to the electrolyte can prevent the abundant metallic Li from being wrapped by insulated SEI.

4. Conclusions

The dead Li⁰ are the major components of inactive Li on the working Li anode, which not only induce the low CE but also hinder the mass transfer of Li⁺ at some sites where the dead Li⁰ accumulates. The formation and evaluation of dead Li⁰ was systematically explored from the processes of electron transfer, conversion of Li⁰ into Li⁺, to Li⁺ diffusion in SEI by adjusting the contact sites of electron channels, the dynamic rate of conversion from Li⁰ to Li⁺ and the structure and component of SEI. According to the above results

and discussion, the design principles of Li anode are proposed to reduce the dead Li⁰ formation as follows: (1) sufficient electron channels to ensure continuous electron transfer to the deposition Li, (2) slow charge transfer rate to guarantee the inter Li⁰ diffusion to the surface of anode, and (3) uniform and fast ion-conducting SEI to prevent the local block of Li⁺ diffusion. This work describes the comprehensive understanding of dead Li⁰ formation and guides to reduce dead Li⁰ for developing the future LMBs with higher CE.

Declaration of Competing Interest

The authors declare that they have no known competing financial interests or personal relationships that could have appeared to influence the work reported in this paper.

Acknowledgments

This work was supported by the Beijing Municipal Natural Science Foundation (Z20J00043), the National Natural Science Foundation of China (21825501), the National Key Research and Development Program (2016YFA0202500), and the Tsinghua University Initiative Scientific Research Program.

Appendix A. Supplementary data

Supplementary data to this article can be found online at <https://doi.org/10.1016/j.jechem.2021.03.048>.

References

- J.M. Thomas, P.P. Edwards, P.J. Dobson, G.P. Owen, *J. Energy Chem.* 51 (2020) 405–415.
- Y. Qin, J. Du, L. Lu, M. Gao, F. Haase, J. Li, M. Ouyang, *Appl. Energ.* 280 (2020) 115957.
- Y.R. Liang, C.Z. Zhao, H. Yuan, Y. Chen, W.C. Zhang, J.Q. Huang, D.S. Yu, Y.L. Liu, M.M. Titirici, Y.L. Chueh, H.J. Yu, Q. Zhang, *InfoMat* 1 (2019) 6–32.
- X.W. Sun, X.Y. Zhang, Q.T. Ma, X.Z. Guan, W. Wang, J.Y. Luo, *Angew. Chem. Int. Ed.* 59 (2020) 6665–6674.
- H.H. Xu, Y.T. Li, A.J. Zhou, N. Wu, S. Xin, Z.Y. Li, J.B. Goodenough, *Nano Lett.* 18 (2018) 7414–7418.
- D. Zhang, S. Wang, B. Li, Y.J. Gong, S.B. Yang, *Adv. Mater.* 31 (2019) 1901820.
- S. Li, M.W. Jjiang, Y. Xie, H. Xu, J.Y. Jia, J. Li, *Adv. Mater.* 30 (2018) 1706375.
- O. Sheng, J. Zheng, Z. Ju, C. Jin, Y. Wang, M. Chen, J. Nai, T. Liu, W. Zhang, Y. Liu, X. Tao, *Adv. Mater.* 32 (2020) 2000223.
- C.J. Niu, H.L. Pan, W. Xu, J. Xiao, J.G. Zhang, L.L. Luo, C.M. Wang, D.H. Mei, J.S. Meng, X.P. Wang, Z. Liu, L.Q. Mai, J. Liu, *Nat. Nanotechnol.* 14 (2019) 594–601.
- Y. Nan, S. Li, Y. Shi, S. Yang, B. Li, *Small* 15 (2019) 1903520.
- B.D. Adams, J.M. Zheng, X.D. Ren, W. Xu, J.G. Zhang, *Adv. Energy Mater.* 8 (2018) 1702097.
- Y. Zhang, T.T. Zuo, J. Popovic, K. Lim, Y.X. Yin, J. Maier, Y.G. Guo, *Mater. Today* 33 (2020) 56–74.
- S. Chen, Y. Xiang, G. Zheng, Y. Liao, F. Ren, Y. Zheng, H. He, B. Zheng, X. Liu, N. Xu, M. Luo, J. Zheng, Y. Yang, *ACS Appl. Mater. Interfaces* 12 (2020) 27794–27802.
- R.H. Wang, W.S. Cui, F.L. Chu, F.X. Wu, *J. Energy Chem.* 48 (2020) 145–159.
- C. Jin, O. Sheng, M. Chen, Z. Ju, G. Lu, T. Liu, J. Nai, Y. Liu, Y. Wang, X. Tao, *Mater. Today Nano* 13 (2021) 100103.
- A. Aryanfar, D.J. Brooks, A.J. Colussi, M.R. Hoffmann, *Phys. Chem. Chem. Phys.* 16 (2014) 24965–24970.
- A.B. Gunnarsdottir, C.V. Amanchukwu, S. Menkin, C.P. Grey, *J. Am. Chem. Soc.* 142 (2020) 20814–20827.
- X. Wang, W. Zeng, L. Hong, W.W. Xu, H.K. Yang, F. Wang, H.G. Duan, M. Tang, H.Q. Jiang, *Nat. Energy* 3 (2018) 227–235.
- Q. Zhao, S. Stalin, C.Z. Zhao, L.A. Archer, *Nat. Rev. Mater.* 5 (2020) 229–252.
- Y.-W. Song, P. Shi, B.-Q. Li, X. Chen, C.-X. Zhao, W.-J. Chen, X.-Q. Zhang, X. Chen, Q. Zhang, *Matter* 4 (2021) 253–264.
- H. Chen, A. Pei, D.C. Lin, J. Xie, A.K. Yang, J.W. Xu, K.X. Lin, J.Y. Wang, H.S. Wang, F.F. Shi, D. Boyle, Y. Cui, *Adv. Energy Mater.* 9 (2019) 1900858.
- Y. Zhang, Y. Shi, X.-C. Hu, W.-P. Wang, R. Wen, S. Xin, Y.-G. Guo, *Adv. Energy Mater.* 10 (2020) 1903325.
- H. Lu, T. Zhang, Y. Kuai, J. Yang, J. Wang, Y. Nuli, Y. Guo, C. Liang, *Energy Storage Mater.* 33 (2020) 452–459.
- R. Xu, X.B. Cheng, C. Yan, X.Q. Zhang, Y. Xiao, C.Z. Zhao, J.Q. Huang, Q. Zhang, *Matter* 1 (2019) 317–344.
- P. Shi, X.-Q. Zhang, X. Shen, B.-Q. Li, R. Zhang, L.-P. Hou, Q. Zhang, *Adv. Funct. Mater.* 31 (2020) 2004189.
- W.L. Huang, N. Zhao, Z.J. Bi, C. Shi, X.X. Guo, L.Z. Fan, C.W. Nan, *Mater. Today Nano* 10 (2020) 100075.
- S. Liu, X. Ji, N. Piao, J. Chen, N. Eidson, J. Xu, P. Wang, L. Chen, J. Zhang, T. Deng, S. Hou, T. Jin, H. Wan, J. Li, J. Tu, C. Wang, *Angew. Chem. Int. Ed.* 60 (2020) 3661–3671.
- R. Pathak, K. Chen, A. Gurung, K.M. Reza, B. Bahrami, J. Pokharel, A. Baniya, W. He, F. Wu, Y. Zhou, K. Xu, Q. Qiao, *Nat. Commun.* 11 (2020) 93.
- X.B. Cheng, R. Zhang, C.Z. Zhao, F. Wei, J.G. Zhang, Q. Zhang, *Adv. Sci.* 3 (2016) 1500213.
- A.B. Gunnarsdottir, S. Vema, S. Menkin, L.E. Marbella, C.P. Grey, *J. Mater. Chem. A* 8 (2020) 14975–14992.
- G. Yasin, M. Arif, T. Mehtab, X. Lu, D.L. Yu, N. Muhammad, M.T. Nazir, H.H. Song, *Energy Storage Mater.* 25 (2020) 644–678.
- X. Zhang, Y.A. Yang, Z. Zhou, *Chem. Soc. Rev.* 49 (2020) 3040–3071.
- C.C. Fang, J.X. Li, M.H. Zhang, Y.H. Zhang, F. Yang, J.Z. Lee, M.H. Lee, J. Alvarado, M.A. Schroeder, Y.Y.C. Yang, B.Y. Lu, N. Williams, M. Ceja, L. Yang, M. Cai, J. Gu, K. Xu, X.F. Wang, Y.S. Meng, *Nature* 572 (2019) 511–515.
- K.H. Chen, K.N. Wood, E. Kazyak, W.S. LePage, A.L. Davis, A.J. Sanchez, N.P. Dasgupta, *J. Mater. Chem. A* 5 (2017) 11671–11681.
- H. Liu, X.B. Cheng, R. Xu, X.Q. Zhang, C. Yan, J.Q. Huang, Q. Zhang, *Adv. Energy Mater.* 9 (2019) 1902254.
- D. Tewari, S.P. Rangarajan, P.B. Balbuena, Y. Barsukov, P.P. Mukherjee, *J. Phys. Chem. C* 124 (2020) 6502–6511.
- Q. Li, B.G. Quan, W.J. Li, J.Z. Lu, J.Y. Zheng, X.Q. Yu, J.J. Li, H. Li, *Nano Energy* 45 (2018) 463–470.
- F.F. Shi, A. Pei, D.T. Boyle, J. Xie, X.Y. Yu, X.K. Zhang, Y. Cui, *Proc. Natl. Acad. Sci. U. S. A.* 115 (2018) 8529–8534.
- C.Y. Fu, V. Venturi, J. Kim, Z. Ahmad, A.W. Ells, V. Viswanathan, B.A. Helms, *Nat. Mater.* 19 (2020) 758–766.
- X.Q. Zhang, X. Chen, X.B. Cheng, B.Q. Li, X. Shen, C. Yan, J.Q. Huang, Q. Zhang, *Angew. Chem. Int. Ed.* 57 (2018) 5301–5305.
- X.B. Cheng, C. Yan, X. Chen, C. Guan, J.Q. Huang, H.J. Peng, R. Zhang, S.T. Yang, Q. Zhang, *Chem* 2 (2017) 258–270.
- C.Z. Zhao, H. Duan, J.Q. Huang, J. Zhang, Q. Zhang, Y.G. Guo, L.J. Wan, *Sci. China Chem.* 62 (2019) 1286–1299.
- A.J. Sanchez, E. Kazyak, Y.X. Chen, K.H. Chen, E.R. Pattison, N.P. Dasgupta, *Acc. Energy Lett.* 5 (2020) 994–1004.
- C. Yan, H. Yuan, H.S. Park, J.Q. Huang, *J. Energy Chem.* 47 (2020) 217–220.
- H. Zhao, J.L. Gu, Y.L. Gao, Q. Hou, Z.Y. Ren, Y.Q. Qi, K. Zhang, C. Shen, J. Zhang, K. Y. Xie, *J. Energy Chem.* 51 (2020) 362–371.
- H.W. Xu, Y. He, Z.B. Zhang, J.L. Shi, P.Y. Liu, Z.Q. Tian, K. Luo, X.Z. Zhang, S.Z. Liang, Z.P. Liu, *J. Energy Chem.* 48 (2020) 375–382.
- Y.X. Yao, X.Q. Zhang, B.Q. Li, C. Yan, P.Y. Chen, J.Q. Huang, Q. Zhang, *InfoMat* 2 (2020) 379–388.
- J.F. Ding, R. Xu, C. Yan, Y. Xiao, Y.R. Liang, H. Yuan, J.Q. Huang, *Chinese Chem. Lett.* 31 (2020) 2339–2342.
- Y.R. Liang, Y. Xiao, C. Yan, R. Xu, J.F. Ding, J. Liang, H.J. Peng, H. Yuan, J.Q. Huang, *J. Energy Chem.* 48 (2020) 203–207.
- Y.T. He, Y.H. Zhang, P. Yu, F. Ding, X.F. Li, Z.H. Wang, Z. Lv, X.J. Wang, Z.G. Liu, X. Q. Huang, *J. Energy Chem.* 45 (2020) 1–6.
- A. Mistry, P.P. Mukherjee, *J. Electrochem. Soc.* 167 (2020) 082510.
- C. Yan, H.R. Li, X. Chen, X.Q. Zhang, X.B. Cheng, R. Xu, J.Q. Huang, Q. Zhang, *J. Am. Chem. Soc.* 141 (2019) 9422–9429.
- X. Shen, X.B. Cheng, P. Shi, J.Q. Huang, X.Q. Zhang, C. Yan, T. Li, Q. Zhang, *J. Energy Chem.* 37 (2019) 29–34.
- D.M. Kang, K. Tang, J. Koh, W.B. Liang, J.P. Lemmon, *J. Energy Chem.* 44 (2020) 68–72.
- F.H. Guo, C. Wu, H. Chen, F.P. Zhong, X.P. Ai, H.X. Yang, J.F. Qian, *Energy Storage Mater.* 24 (2020) 635–643.
- B.Q. Li, X.R. Chen, X. Chen, C.X. Zhao, R. Zhang, X.B. Cheng, Q. Zhang, *Research* 2019 (2019) 4608940.
- Z.Y. Yao, W.S. Jia, Z.H. Wang, J. Ruan, X.G. Kong, X. Guan, Z.H. Wang, J.Z. Li, Y. Wang, W. Zou, F. Zhou, *J. Energy Chem.* 51 (2020) 285–292.
- K. Wu, B.L. Zhao, C.K. Yang, Q. Wang, W. Liu, H.H. Zhou, *J. Energy Chem.* 43 (2020) 16–23.
- J. Liu, H. Yuan, X. Tao, Y. Liang, S.J. Yang, J.-Q. Huang, T.-Q. Yuan, M.-M. Titirici, Q. Zhang, *EcoMat* 2 (2020) e12019.
- H.D. Yuan, J.W. Nai, Y.J. Fang, G.X. Lu, X.Y. Tao, X.W. Lou, *Angew. Chem. Int. Ed.* 59 (2020) 15839–15843.
- X.B. Cheng, C.Z. Zhao, Y.X. Yao, H. Liu, Q. Zhang, *Chem* 5 (2019) 74–96.
- X.Q. Zhang, T. Li, B.Q. Li, R. Zhang, P. Shi, C. Yan, J.Q. Huang, Q. Zhang, *Angew. Chem. Int. Ed.* 59 (2020) 3252–3257.
- X.R. Chen, Y.X. Yao, C. Yan, R. Zhang, X.B. Cheng, Q. Zhang, *Angew. Chem. Int. Ed.* 59 (2020) 7743–7747.
- C. Yan, R. Xu, J.L. Qin, H. Yuan, Y. Xiao, L. Xu, J.Q. Huang, *Angew. Chem. Int. Ed.* 58 (2019) 15235–15238.